

1 High-frequency variability in the  
2 North Icelandic Jet

3 B. E. Harden<sup>1</sup> and R. S. Pickart

4 Woods Hole Oceanographic Institution, Woods Hole, USA

5 June 19, 2018

<sup>1</sup>Woods Hole Oceanographic Institution, 266 Woods Hole Road, Woods Hole, MA 02543.  
bharden@whoi.edu

**ABSTRACT**

7        We describe the high-frequency variability in the North Icelandic Jet (NIJ) on the  
8    Iceland Slope using data from the densely instrumented Kögur mooring array deployed  
9    upstream of the Denmark Strait sill from September 2011 to July 2012. Significant sub-8-  
10   day variability is ubiquitous in all moorings from the Iceland slope with a dominant period  
11   of 3.6 days. We attribute this variability to topographic Rossby waves on the Iceland slope  
12   with a wavelength of  $62 \pm 3$  km and a phase velocity of  $17.3 \pm 0.8$  km day<sup>-1</sup> directed  
13   downslope ( $-9^\circ$  relative to true-north). We test the theoretical dispersion relation for these  
14   waves against our observations and find good agreement between the predicted and mea-  
15   sured direction of phase propagation. We additionally calculate a theoretical group veloc-  
16   ity of 36 km day<sup>-1</sup> directed almost directly up-slope ( $138^\circ$  relative to true-north) which  
17   agrees well with the propagation speed and direction of observed energy pulses. We use  
18   an inverse wave tracing model to show that this wave energy is generated locally, offshore  
19   of the array, and does not emanate from the upstream or downstream directions along the  
20   Iceland slope. It is hypothesized that either the meandering Separated East Greenland Cur-  
21   rent located seaward of the NIJ, or intermittent aspiration of dense water into the Denmark  
22   Strait Overflow, are the drivers of the topographic waves.

## 23 1. Introduction

24 The Denmark Strait Overflow is the major pathway of dense water out of the Nordic  
25 Seas. It transports 3.2 Sv, or approximately 50%, of the total outflow (Dickson and Brown,  
26 1994; Jochumsen *et al.*, 2017), and hence plays a crucial role in the Atlantic meridional  
27 overturning circulation (AMOC). While the existence of this overflow has been known  
28 for many decades, our understanding of the processes that govern it and the underlying  
29 dynamics remains incomplete. One important aspect that requires further study is deter-  
30 mining the upstream sources of the dense water and how it approaches the sill. If we are to  
31 determine how a changing climate might impact the AMOC, we need to understand bet-  
32 ter the connection between the water mass transformation process and the flux of newly  
33 ventilated water to Denmark Strait.

34 Most of the Denmark Strait Overflow water (approximately 70%) comes from the  
35 East Greenland Current by way of the Nordic Seas boundary current system (Våge *et al.*,  
36 2013; Harden *et al.*, 2016) (see Figure 1). Specifically, warm Atlantic inflow across the  
37 Greenland-Scotland Ridge is progressively cooled as it flows northward towards Fram  
38 Strait, much of it recirculating in the strait and subducting to mid-depth (Mauritzen, 1996).  
39 This is joined by Atlantic water exiting the strait that has circumnavigated the Arctic, and  
40 together the transformed Atlantic water flows southward in the East Greenland Current.  
41 As the current rounds Scoresby Sund, it splits into two branches (Figure 1). One continues  
42 towards the sill as a shelfbreak jet (Håvik *et al.*, 2017). The other carries approximately  
43 60% of the East Greenland Current water out into the central strait via eddies and/or gyre-  
44 like deflections of the shelfbreak jet (Våge *et al.*, 2013; Harden *et al.*, 2016). This interior  
45 pathway, known as the separated East Greenland current, then flows into the strait along  
46 the outer Iceland slope.

47 The remaining 30% of Denmark Strait Overflow water is supplied by the North Ice-  
48 landic Jet (NIJ), a more recently discovered branch of the upstream circulation (Jonsson  
49 and Valdimarsson, 2004; Våge *et al.*, 2011). This mid-depth intensified jet advects waters

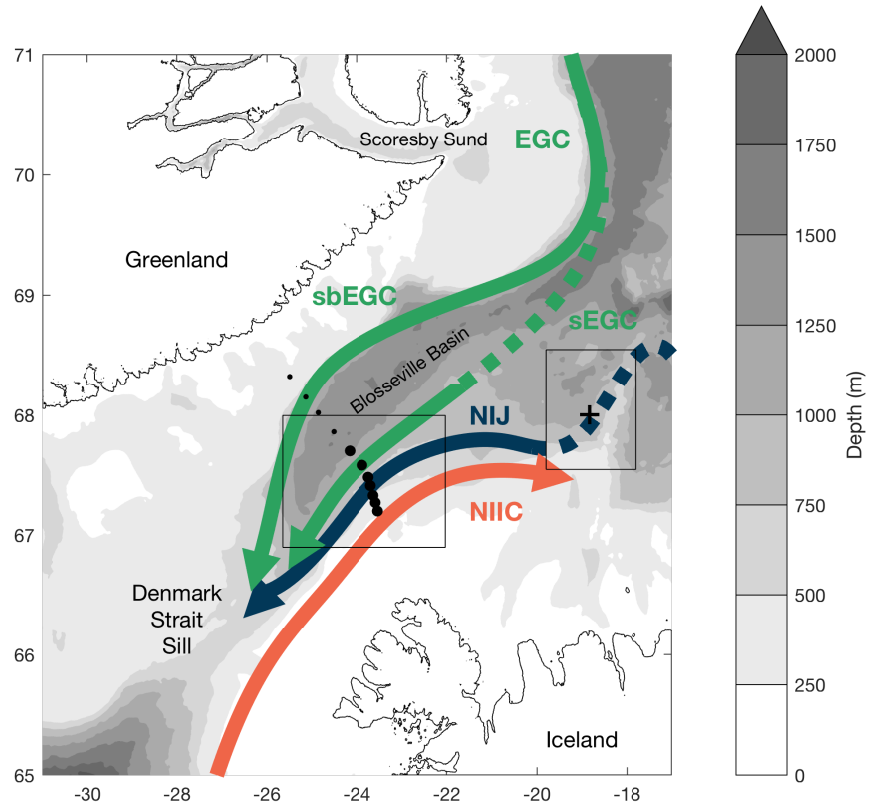


Figure 1: Map of the study region showing the overflow pathways approaching the Denmark Strait Sill: the North Icelandic Jet (NIJ) and the two East Greenland Current (EGC) pathways, one along the shelfbreak (sbEGC) and the other in a separated branch on the Iceland Slope (sEGC). Dashed portions show parts of pathways that still need further clarification. Also shown is the northward flowing surface-intensified current, the North Icelandic Irminger Current (NIIC). Black dots show the locations of the moorings in the Kögur array with larger dots indicating the subset of seven moorings used in this study. The upstream cross is the mooring to the west of the Kolbeinsey ridge referred to in the text. The bathymetry is from IBCAO v3. The inset boxes are the domains shown in Figures 4 (left) and 7 (right).

50 distinct from those found in the East Greenland Current (colder and fresher) suggestive of  
51 a source in the central Iceland or Greenland seas (Våge *et al.*, 2011; 2015; Harden *et al.*,  
52 2016). The NIJ contains the densest water that feeds the overflow; its waters are found in  
53 the deepest part of the sill (Mastropole *et al.*, 2017) and subsequently sink to the deepest  
54 depths in the core of the overflow.

55 The leading hypothesis for the formation of the NIJ, supported by both models and  
56 observations, is that it represents the lower limb of a local overturning cell in the Iceland  
57 sea (Våge *et al.*, 2011; Behrens *et al.*, 2017). The upper limb of the cell is the North  
58 Icelandic Irminger Current (NIIC), which sheds warm water into the Iceland Sea that is  
59 cooled by air-sea heat loss. The transformed water then returns southward towards the  
60 boundary where it sinks and forms the NIJ. However, many questions remain unanswered  
61 about this proposed system. For instance, the winter mixed-layers in the Iceland Sea don't  
62 appear to be dense enough to account for the deepest water in the NIJ (Våge *et al.*, 2015),  
63 whereas those in the Greenland Sea do (Strass *et al.*, 1993; Rudels *et al.*, 2002).

64 Regardless of the source of the NIJ, it clearly constitutes a vital component of the  
65 circulation upstream of the sill. Harden *et al.* (2016) investigated the jet's mean and sea-  
66 sonal contribution to the overflow, demonstrating that there is time-dependent partitioning  
67 of transport between the NIJ and the other two overflow branches on weekly to monthly  
68 timescales, likely driven by the wind. Pickart *et al.* (2017) noted that the NIJ appears to  
69 be coupled to the northward-flowing NIIC and that, on occasion, it consists of multiple  
70 branches. Using historical hydrographic data, Pickart *et al.* (2017) also revealed a clear  
71 link between the interannually varying properties of the NIJ and those of the densest water  
72 at the Denmark Strait sill, leaving little doubt that the NIJ is a major source of the overflow  
73 plume.

74 It has long been known that the Denmark Strait Overflow varies on short (order days)  
75 timescales (Smith, 1976; Bruce, 1995; Käse *et al.*, 2003). Some of this variability is  
76 associated with the passage of lenses of cold, dense, overflow water referred to as boluses

77 (Cooper, 1955). Recently, von Appen *et al.* (2017) identified a second type of mesoscale  
78 feature in the strait that was termed a pulse. In contrast to boluses, pulses correspond to  
79 a thinning of the overflow layer associated with a large increase in equatorward velocity.  
80 Both of these features have been identified in a high-resolution regional model as well  
81 (Almansi *et al.*, 2017). von Appen *et al.* (2017) showed that, taking into account both  
82 boluses and pulses, a mesoscale feature passes through Denmark Strait on average every  
83 2 days. Presently, however, it is unknown if these disturbances originate from upstream or  
84 if they are associated with local dynamics near the sill.

85 The goal of the present study is to shed light on some of the above processes by de-  
86 scribing the high frequency variability of the NIJ north of the Denmark Strait. We use  
87 timeseries data from a year-long mooring array that was maintained roughly 200 km up-  
88 stream of the sill (Figure 1). This is the same data set used by Harden *et al.* (2016) to inves-  
89 tigate the mean and seasonal attributes of the NIJ. While Harden *et al.* (2016) mentioned  
90 that the NIJ exhibits high-frequency variability, they did not elaborate on this. We begin  
91 with a brief description of the data, followed by a characterization of the high-frequency  
92 signal. We discuss how this signal is consistent with the existence of topographic Rossby  
93 waves on the Iceland slope, and then investigate the source region of the energy in these  
94 waves through inverse wave tracing.

## 95 **2. Data and Methods**

96 The data for this study come from the densely instrumented Kögur mooring array  
97 spanning the Denmark Strait approximately 200 km upstream of the sill. The array was  
98 deployed for 11 months from September 2011 to July 2012 and consisted of 12 moorings  
99 (named KGA 1-12) equipped with instrumentation to measure both the hydrography and  
100 velocity of the water column from 50 m to the bottom. Harden *et al.* (2016) present a  
101 detailed description of the mooring data, including the instrumentation, processing steps,  
102 and sensor accuracies. The array captured the majority of the overflow water ( $\sigma_\theta > 27.8$

103  $\text{kg m}^{-3}$ ) passing through the northern part of the strait towards the sill.

104 Here we use primarily the gridded product described in Harden *et al.* (2016), which  
105 has a lateral resolution of 8km and vertical resolution of 50 m. Because of our focus  
106 on the Iceland slope, we consider a subset of these data up to and including the location  
107 of mooring KGA 7, approximately 70 km offshore of the Iceland shelfbreak. The mean  
108 velocity sections demonstrate that this portion of the array captures both the NIJ and the  
109 majority of the Separated EGC (Figure 2). For parts of the analysis we also use the data  
110 on a mooring-by-mooring basis. All of the velocities have been subjected to a 36-hour  
111 low-pass butterworth filter to remove the predominant M2 tidal constituent.

112 Additional data come from a mooring located approximately 200 km upstream of the  
113 Kögur Array on the west side of the Kolbeinsey Ridge ( $68^{\circ}00'N$ ,  $18^{\circ}50'W$ , see Figure  
114 1) This was deployed on the 1000 m isobath from September 2007 to mid-October 2008  
115 and consisted of a McLane Moored Profiler and acoustic current meter providing profiles  
116 between 100 m and the bottom twice-daily. As with the Kögur data, we low-passed the  
117 velocity timeseries using a 36-hr filter to remove the M2 tidal component of the flow.  
118 These data are described in greater detail by Jónsson and Valdimarsson (2012).

119 The inverse wave tracing of topographic Rossby waves (TRWs) was done using the  
120 model described by Meinen *et al.* (1993) and implemented by Pickart (1995) for investi-  
121 gating TRWs in the Deep Western Boundary Current off of Cape Hatteras, North Carolina.  
122 The method uses the TRW dispersion relation (Equation 2) to calculate the group veloc-  
123 ity (Equations 3 and 4) and then backtracks the evolution of the wave with a time step  
124 of 30 minutes. The wave parameters and dispersion relation are recalculated at each step  
125 for the local bottom depth, bottom slope, and water column stratification. A new group  
126 velocity is then found and used to further trace the wave. In addition, given that the calcu-  
127 lated group velocities of the waves are comparable to the magnitude of the mean flow, we  
128 also correct the propagation paths for the mean velocities (calculated as a function of the  
129 underlying bathymetry).

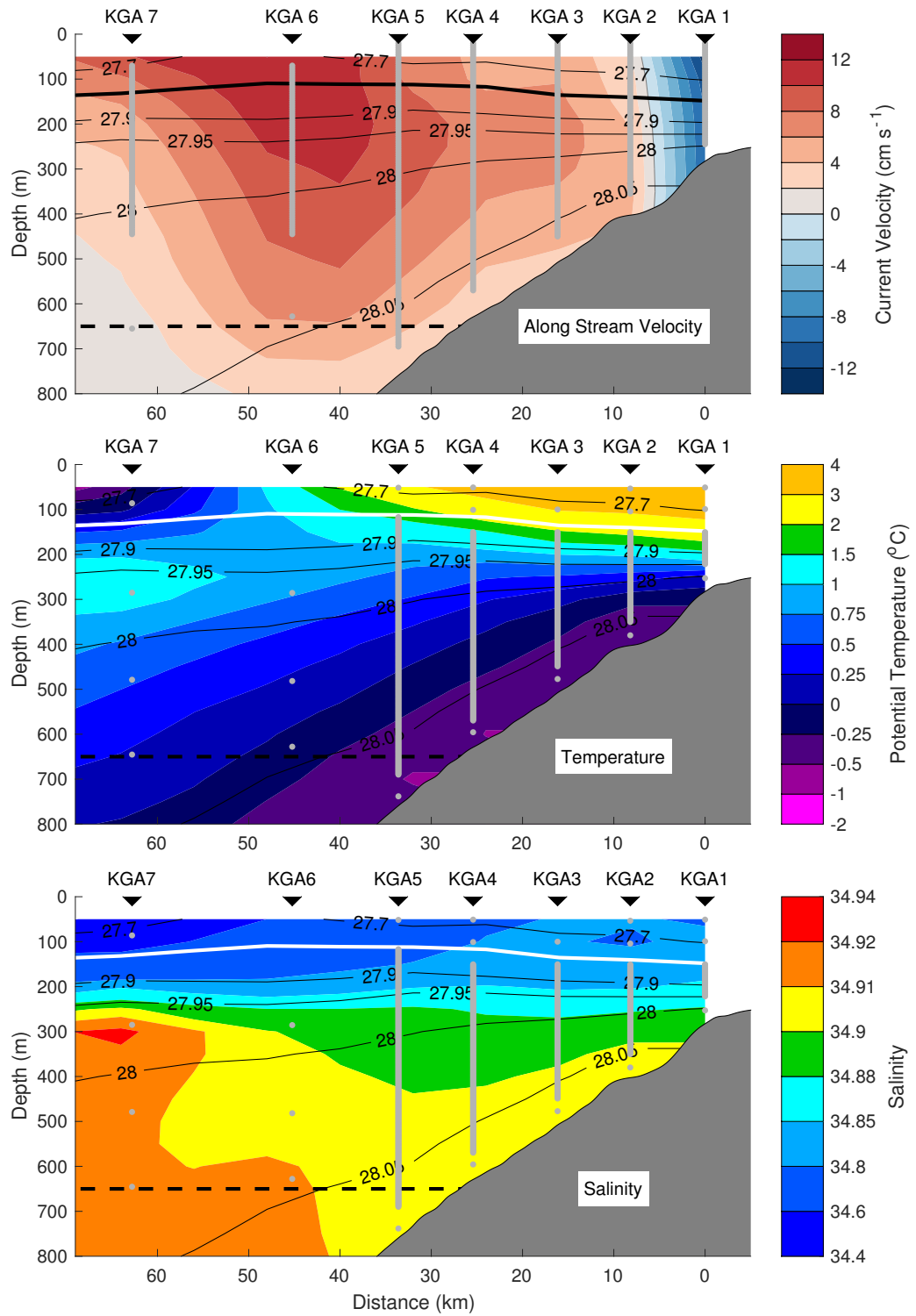


Figure 2: Mean vertical section of the along-stream (cross-transect) velocity (top), and median sections of potential temperature (middle) and salinity (bottom) for the 11-month period of the Kögur array. Overlaid in black contours on each panel is the mean density with the  $27.8 \text{ kg m}^{-3}$  isopycnal (the upper boundary of Denmark Strait Overflow Water) highlighted. The viewer is looking to the northeast with Iceland on the right. Positive velocities are equatorward. The horizontal black dashed line indicates the depth of the Denmark Strait sill. The moorings (black triangles) are labeled, and the average instrument locations are shown by the grey points. The bathymetry is from a shipboard echosounder.



130 Most of the required input parameters for the inverse wave tracing model come di-  
131 rectly from the moored data and are the same as those used for the theoretical TRW  
132 dispersion relation calculations (see Section 3.a.). For the bathymetry we used the In-  
133 ternational Bathymetric Chart of the Arctic Ocean 30-arcsec gridded product (Jakobsson  
134 *et al.*, 2012). To remove seamounts and other sharp topographic features we smoothed the  
135 bathymetry using a filter of 60 km (comparable to our measured TRW wavelength). In  
136 contrast to Pickart (1995) who subsequently fit splines to the data to be able to find the  
137 bottom depth and gradients at any location, we deemed our resolution to be high enough  
138 (and our smoothing window great enough) to simply use linear interpolation. The total  
139 integration period for the wave tracing was 48 hours.

### 140 **3. Results**

141 As discussed in Harden *et al.* (2016), the vertical sections of velocity and hydrography  
142 at the Kögur site show the signatures of both the NIJ and the Separated EGC. However, in  
143 the mean the two features are merged to some degree and hence do not appear as distinct  
144 cores (Figure 2). Previous synoptic sections (Våge *et al.*, 2011) and the water mass prop-  
145 erties recorded in this array allow us to visualize this system as two currents though. The  
146 NIJ is on the upper Iceland slope and is characterized by a mid-depth intensified flow car-  
147 rying the coldest, densest overflow water banked up on the slope. The Separated EGC is  
148 farther offshore; its key features are a surface intensification and the transport of warmer,  
149 saltier overflow water at approximately 300 m. In the mean section the transition between  
150 the currents occurs at approximately 35 km offshore (Figure 2), although synoptically the  
151 two currents are often completely separate (Harden *et al.*, 2016). Inshore of the NIJ, on  
152 the Iceland shelf, is the poleward flowing North Icelandic Irminger Current (NIIC, see also  
153 Figure 1).

154 The two overflow currents vary strongly on short timescales. This is evident by con-  
155 sidering the timeseries of depth-averaged alongstream and cross-stream velocities, which

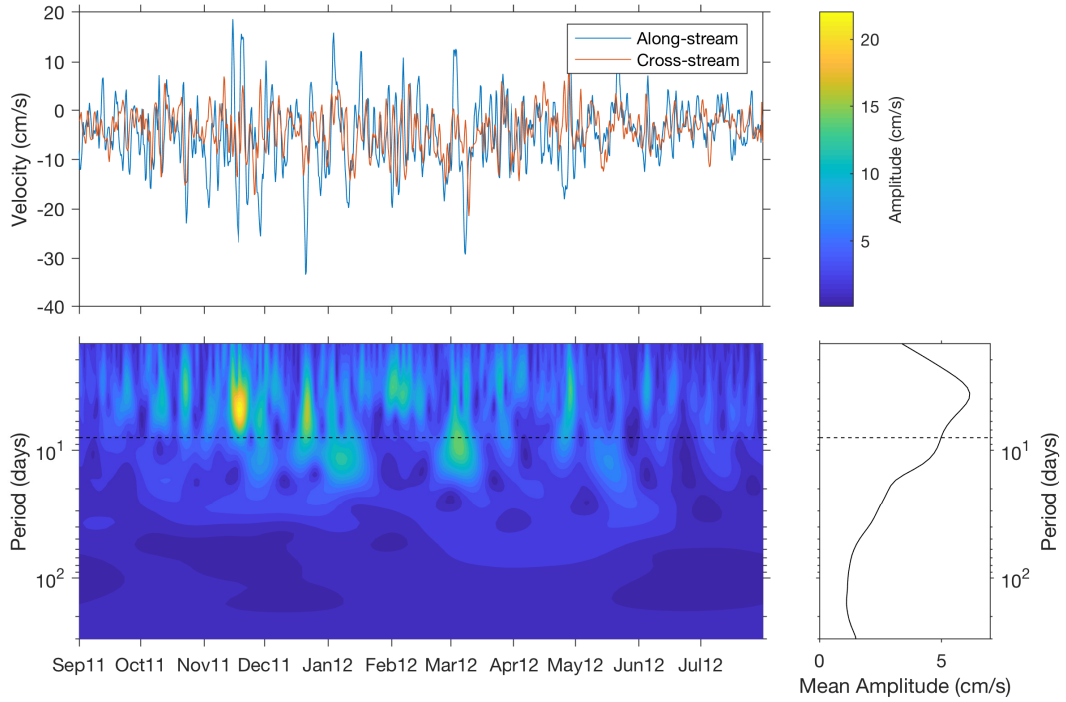


Figure 3: Top: Depth-averaged along-stream (blue) and cross-stream (red) components of velocity for the grid point closest to mooring KGA 3. Bottom left: Wavelet spectrum of the depth-averaged velocity. This was done using the jLab toolbox (Lilly, 2017) with standard Morlet wavelets with  $\gamma=3$  and  $\beta = 2$ . The color scale for this plot is at the top right. Bottom right: Mean wavelet amplitude for the length of the deployment. The dashed line in the bottom panels indicates the 8-day cut-off period for the high-pass filter used in the study.

156 is shown for the mooring in the core of the NIJ in Figure 3(a). To quantify this high fre-  
 157 quency variability we computed the wavelet spectrum of the depth-averaged velocity using  
 158 Morlet wavelets (Lilly, 2017). This is shown for the NIJ mooring in Figure 3(b). One sees  
 159 that the signal is concentrated at sub-8-day periods with a maximum average energy at 3.6  
 160 days. As such, we high-passed the velocity timeseries using a 8-day butterworth filter<sup>1</sup>

161 The high-passed current ellipses for each mooring are useful for characterizing differ-  
 162 ent regimes across the array (Figure 4). In the NIIC (KGA 1), the current ellipse is elon-  
 163 gated in the direction of the mean flow indicative of a current pulsing along its axis. By  
 164 contrast, within the Separated EGC (KGA 6 and 7), the elongation of the current ellipses

<sup>1</sup>Different period filters were implemented, ranging in length from 4 days to 30 days, but the 8-day filter was most effective in isolating the peak high-frequency energy.

165 is perpendicular to the mean flow demonstrating that this current meanders. However, in  
 166 the NIJ (KGA 2-4), the major axes of the current ellipses are aligned at an oblique angle to  
 167 both the mean flow and the underlying bathymetry. This is characteristic of TRWs (Pickart  
 168 and Watts, 1990). KGA 5 appears to be in a transition region between conditions in the  
 169 NIJ and those in the Separated EGC.

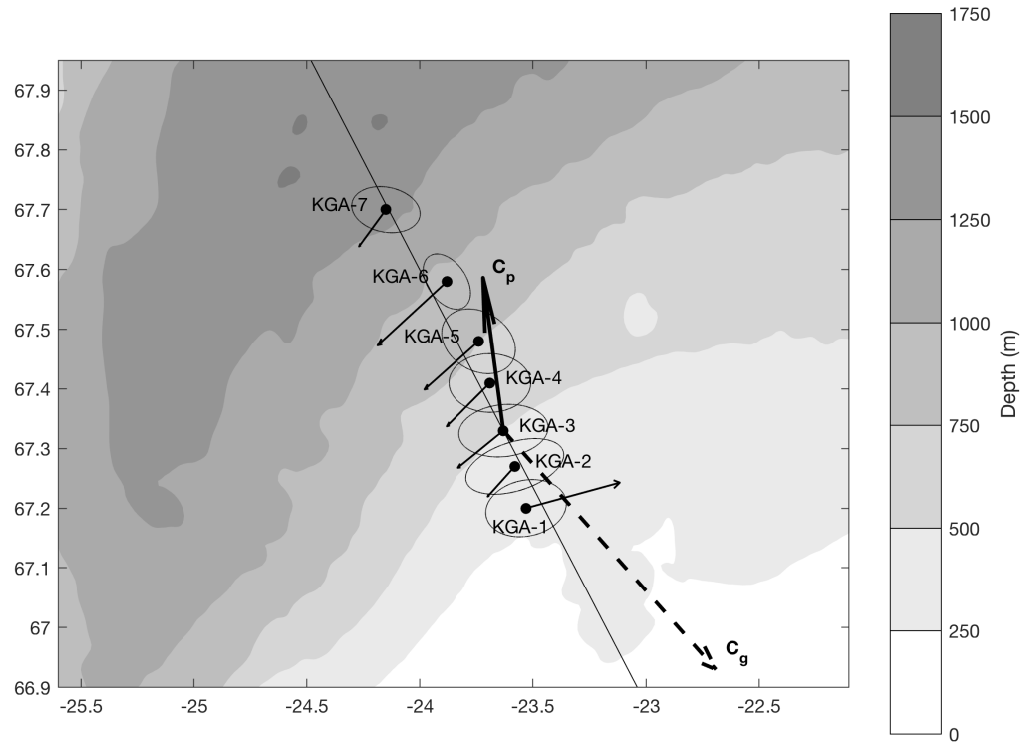


Figure 4: Aspects of the flow measured by the Kögur moorings (black circles). The thin vectors indicate the mean velocity averaged from 100 m to the depth of the ADCP at each mooring (see gray lines in Figure 2). Also shown are the 8-day high-passed current ellipses for the same depth range. The thick black arrow ( $C_p$ ) denotes the direction of TRW phase propagation averaged over KGA 2-4 (plotted at KGA 3). The dashed black arrow shows the direction of TRW group velocity ( $C_g$ ). All vectors and current ellipses are drawn to the same scale as indicated. The long black line is the mean downslope direction averaged between KGA 2-4. The bathymetry is from IBCAO v3.

170 Another perspective of the high-frequency variability present across the array is ob-  
 171 tained by computing Hovmöller plots. We did this for the depth-mean along-stream veloc-

ity, which is shown in Figure 5a. On the Iceland slope (inshore of approximately 50 km), the sub-8-day period signal dominates throughout the record. Farther offshore, however, in the vicinity of the Separated EGC, there is also a lower frequency signal on timescales of weeks to months. These more slowly varying fluctuations were described by Harden *et al.* (2016) and attributed in part to the time-varying upstream bifurcation of the EGC. We now investigate the nature of the sub-8-day variability.

#### *a. Topographic Rossby Waves*

We resolved the sub-8-day depth-averaged flow in the gridded product along the major axis of the current ellipses at each offshore location. Particularly in the NIJ, the variability along these axes have a sinusoidal form and are lagged between moorings such that the pulses of current progress offshore in time (Figure 5b). This implies a downslope phase propagation of this variability.

We argue that this is the signature of TRWs. These waves are supported by topographic  $\beta$  and result in transverse fluctuations that are often at an oblique angle to the mean flow (recall the orientation of the 8-day variance ellipses in the vicinity of the NIJ, Figure 4). TRWs are found in many slope regions of the world’s oceans (Garrett, 1979; Louis *et al.*, 1982; Pickart and Watts, 1990). Key features of TRWs include wave vectors (and hence phase velocities) that are perpendicular to the velocity variability, a group velocity which is at an oblique angle to the phase velocity, and a tendency to be bottom-trapped in regions of significant stratification.

Given that the phase propagation is perpendicular to the velocity variability, we deduce that the wave phase is progressing downslope at  $-9^\circ\text{T}$  (where  $^\circ\text{T}$  refers to degrees relative to true north). This value is the average direction over KGA 2–4, where we see the most direct evidence for TRWs (see Figure 4). Following Pickart and Watts (1990), we then calculated the phase speed over the range of moorings KGA 2–4 using,

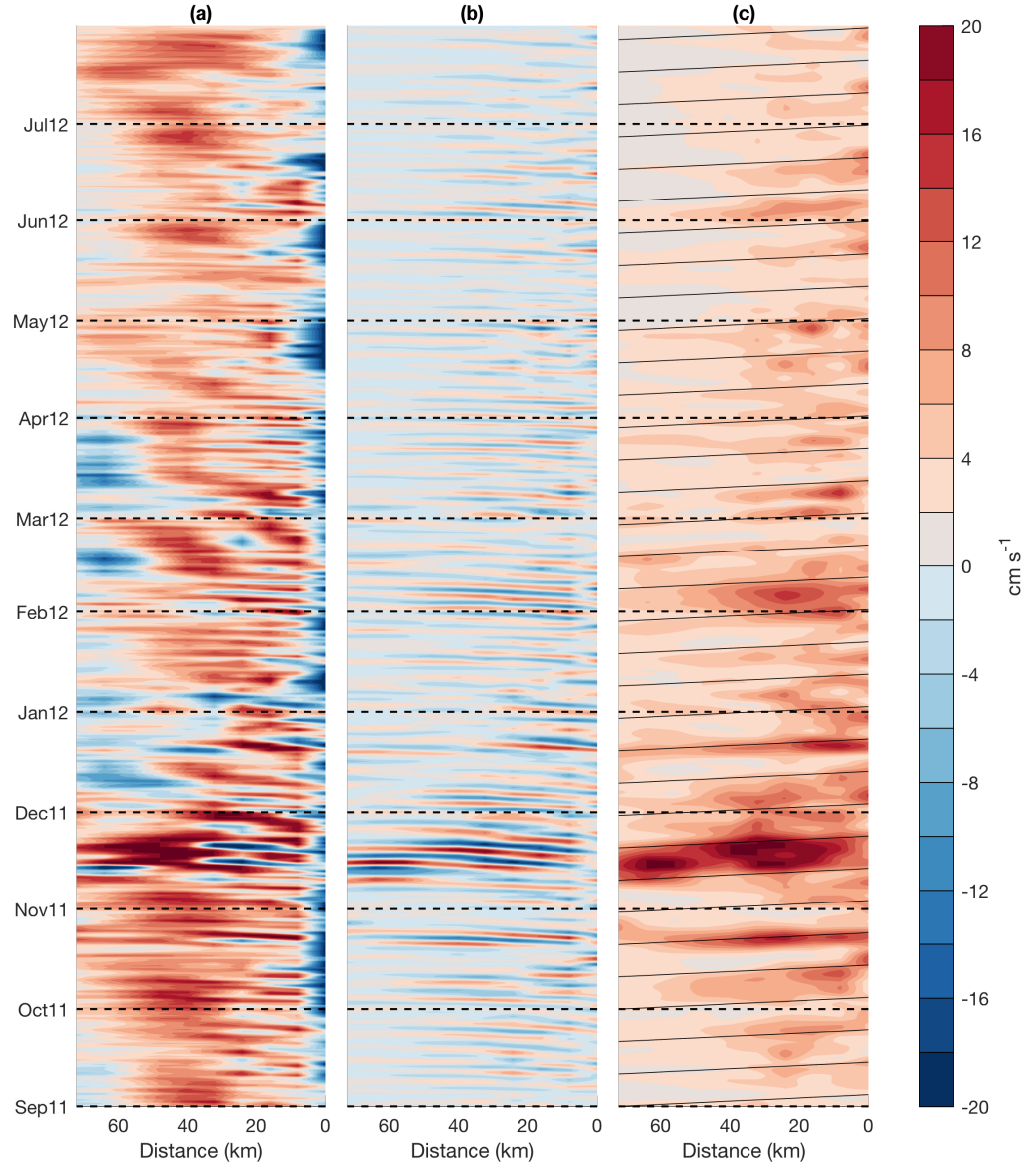


Figure 5: Hovmöller plots from the gridded mooring data of a) the depth-mean along-stream velocity (below 100 m, same for all plots); b) the 8-day high-passed, depth-mean component of velocity in the direction of the major axis of the local current ellipse; and c) the wavelet amplitude at a 4-day period for the depth-mean velocity. Iceland is to the right of each panel as in Figure 2. The sloped, black guidelines in panel c are angled at the theoretical group velocity for the measured topographic Rossby waves (see text for details).

$$c_p = \frac{1}{T} \frac{360}{\bar{\phi}} \frac{\bar{\Delta S}}{\cos(\Delta)} \quad (1)$$

where  $T$  is the wave period ( $= 3.6$  days),  $\bar{\phi}$  is the average phase offset ( $= 48 \pm 3^\circ$ ),  $\bar{\Delta S}$  is the average instrument spacing ( $= 8.1 \pm 0.2$  km), and  $\Delta$  is the angle between the mooring array and the direction of wave propagation ( $= 8 \pm 4^\circ$ ). This equation is essentially a geometric calculation that adjusts the wave propagation speed observed between moorings to being along the wave vector instead.

The resulting phase speed is  $17.3 \pm 0.8$  km day $^{-1}$  corresponding to a wavelength of  $62 \pm 3$  km. The error estimates arise in equal contributions from uncertainties in  $\bar{\phi}$ ,  $\bar{\Delta S}$ , and  $\Delta$ .

As a consistency check that the observed fluctuations are in fact TRWs, we can employ the TRW dispersion relation for waves in a uniformly stratified ocean over a linearly sloping bottom, with a rigid lid and neglecting planetary  $\beta$ . This result is derived in non-dimensional units in Pedlosky (1979) and can be written in dimensional units (following Pickart (1995)) as:

$$T = \frac{2\pi \tanh\left(\frac{2\pi ND}{\lambda f}\right)}{N\Gamma \sin(\theta)} \quad (2)$$

where  $T$  is the period of the wave (3.6 days),  $N$  is the average water column Brunt Väisälä frequency ( $= 3.3 \times 10^{-5}$ , averaged using the gridded data below 100 m),  $D$  is the depth ( $= 500$  m),  $\lambda$  is the scalar wavelength (62 km),  $f$  is the Coriolis parameter ( $= 1.35 \times 10^{-4}$ ),  $\Gamma$  is the bottom slope ( $= 0.016$ , from IBCAO v3), and  $\theta$  is the phase velocity direction relative to downslope.

Using Equation 2 we obtain a predicted value of  $\theta = 29^\circ$  using our knowledge of the other variables. This predicted value compares well with the measured value of  $24^\circ$  (from

the average downslope angle between moorings KGA 2–4). There is of course uncertainty in the measured downslope angle depending on the region selected for the averaging. For example, if we expand the calculation of the downslope direction to encompass KGA 1–5, the measured  $\theta$  becomes  $33^\circ$ , which still agrees well with the predicted value. In addition, the bottom-trapping scale ( $=f/Nk$ ) is much greater than 1000 m, in agreement with the observed velocities which are largely barotropic.

All of this supports our assertion that the dominant high-frequency variability in the NIJ is due to TRWs. The obvious question is, where and how are these waves being generated? Using the dispersion relation we can calculate the group velocity ( $C_g$ ), which can be written as:

$$C_{gx} = \frac{\partial \sigma}{\partial k} = N\Gamma \left( \frac{\lambda \cos^2 \theta}{2\pi \tanh(\frac{2\pi ND}{\lambda f})} + \frac{ND \sin^2 \theta}{f \sinh^2(\frac{2\pi ND}{\lambda f})} \right), \quad (3)$$

$$C_{gy} = \frac{\partial \sigma}{\partial l} = -\frac{1}{2} N\Gamma \sin(2\theta) \left( \frac{\lambda}{2\pi \tanh(\frac{2\pi ND}{\lambda f})} + \frac{ND}{f \sinh(\frac{2\pi ND}{\lambda f})} \right) \quad (4)$$

where the  $x$  and  $y$  subscripts are for the group velocities in the along-slope (positive equatorward) and cross-slope (positive up-slope) directions, respectively,  $k$  and  $l$  are the wave vectors in the  $x$  and  $y$  directions, and  $\sigma$  is the angular frequency of the wave ( $=2\pi/T$ ). The rest of the parameters are defined above for Equation 2.

For the observed parameters, we find the magnitude of the group velocity to be  $36 \text{ km day}^{-1}$  directed almost directly up-slope at the array site ( $138^\circ\text{T}$ , see Figure 4). This implies that the energy source lies offshore. We can corroborate this onshore propagation of energy observationally by considering the wavelet amplitude for the 4-day signal at each mooring site. The Hovmöller plot in Figure 5c shows clear occurrences of onshore energy propagation that are in line with the predicted group velocity, which contrasts with the offshore phase propagation in Figure 5b. Particularly good examples of this onshore energy propagation occur in mid-November, late December, early February, and early

239 June.

240 *b. Wave Tracing and TRW Formation Mechanisms*

241 In order to shed light on the source of the TRWs, we implemented the inverse wave  
242 tracing model described in Section 2. In particular, we calculated the wave paths back-  
243 wards in time from moorings KGA 2–5. For each mooring, the model was initialized  
244 with the local wavenumber (assuming constant phase velocity and wave period across the  
245 array). Since KGA 5 only marginally displayed TRW behavior, the results from that moor-  
246 ing should be considered less robust. As stated in Section 2, we also incorporate the mean  
247 flow into our wave tracing which impacts the inverse traces to some extent (bends them in  
248 the upstream direction).

249 The calculated paths indicate that the waves originate offshore of the moorings in the  
250 vicinity of the deep Blosseville Basin (Figure 6). The traces from KGA2–4 converge in  
251 a relatively localized region directly downslope of the array, while the trace from KGA5  
252 (less robust) has a slight upstream deflection. It is clear that the TRW energy does not  
253 emanate from either the Denmark Strait or from upstream in the Iceland Sea, but instead  
254 originates locally.

255 TRWs are a ubiquitous feature in the middle Atlantic Bight between Cape Hatteras,  
256 North Carolina and the Grand Banks of Newfoundland (Louis *et al.*, 1982; Johns and  
257 Watts, 1986; Pickart and Watts, 1990). The source of the waves appears to be the Gulf  
258 Stream. Both Hogg (1981) and Schultz (1987) argued that TRWs observed along the US  
259 continental slope emanated from large amplitude Gulf Stream meanders offshore. Louis  
260 *et al.* (1982) made the case that bursts of TRWs measured south of Nova Scotia resulted  
261 from Gulf Stream eddy formation. Pickart (1995) demonstrated that the TRWs observed  
262 near Cape Hatteras were forced by meanders of the Gulf Stream as it flowed over a bend  
263 in topography farther to the east.

264 In light of these studies, it is natural to suspect that the TRWs measured at the Kögur  
265 array site are generated by the Separated EGC. This current is energetic, and, as noted



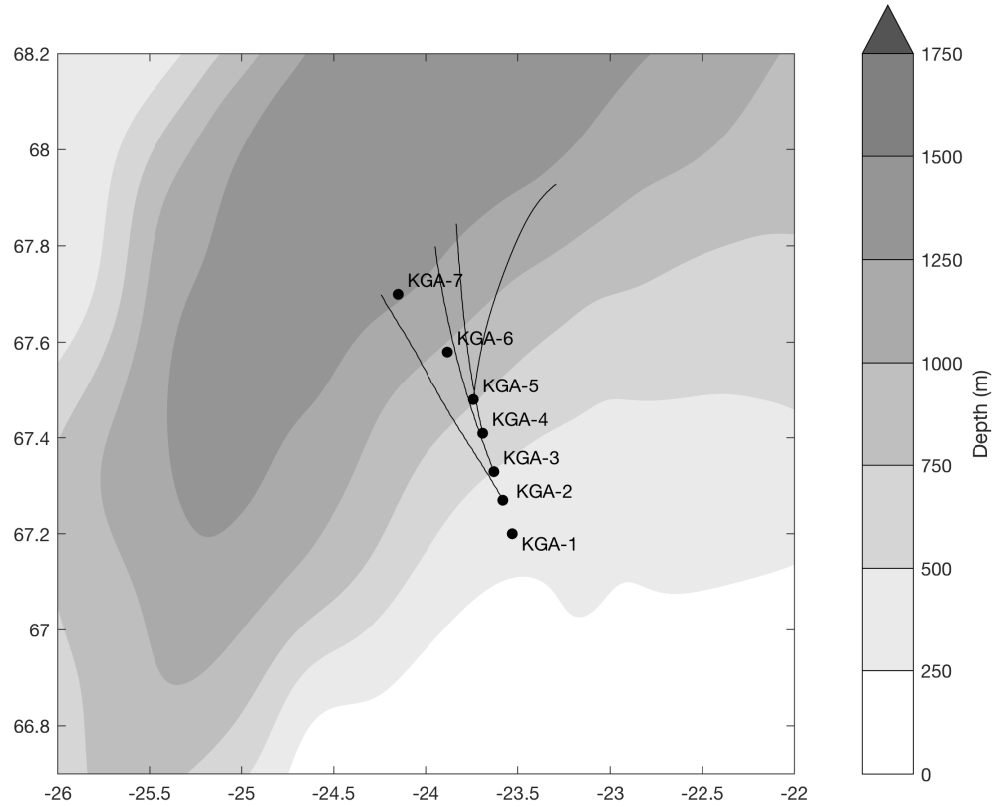


Figure 6: Ray paths of the Topographic Rossby Waves (thin lines) computed using the inverse wave tracing model for moorings KGA 2-5. Wave traces are truncated as they pass the 1300 m isobath. The bathymetry is from IBCAO v3 smoothed over 60 km (see text for details).

266 above, is subject to meandering (akin to the Gulf Stream). The wave tracing indicates that  
267 the TRW energy emanates from the Blosseville Basin where the Separated EGC resides.  
268 Additionally, there is evidence in Figure 5c that times of strong TRW activity on the upper  
269 slope are often preceded by increases in meander energy in the Separated EGC. Recall  
270 that the velocities in Figure 5b,c are rotated along the major axis of the local variance  
271 ellipse (see Figure 4), hence they represent meanders offshore in the Separated EGC and  
272 TRWs onshore in the NIJ. Therefore, the signal propagation seen in Figure 5c (for example  
273 in late-October, mid-November, late-December and early-February) can be interpreted as  
274 offshore meanders transferring energy onshore into TRWs.

275 Another possible trigger for the waves is the intermittent aspiration of deeper waters  
276 towards the Denmark Strait Sill. Harden *et al.* (2016) demonstrated that 0.6 Sv of the  
277 overflow transport approaching the sill does so from below sill depth, which necessarily  
278 must climb a topographic gradient to reach the sill. Further to that study, we also observe  
279 variability below sill depth that is aligned obliquely across the Strait (not shown) which  
280 is correlated to the TRW variability on the Iceland Slope. It is unclear at this stage what  
281 is driving this deep variability. It may be a deep-reaching expression of the meandering  
282 Separated EGC, wave signals from the Denmark Strait Overflow downstream, or a com-  
283 bination of both. As we will touch upon in Section 4, a complete understanding of the  
284 linkages between the variability at the sill and the full Kögur Array (all 12 moorings) will  
285 likely be necessary to definitely determine the source of deep energy in the Blosseville  
286 Basin.

287 Regardless of the formation mechanism, the presence of TRWs in our data raises the  
288 question of whether they are present along the entire Iceland slope or instead unique to our  
289 sampling region. To address this we examined the velocity data from a mooring deployed  
290 approximately 200 km upstream on the Iceland slope near the Kolbeinsey Ridge from  
291 2007–2008 (Figure 7).

292 The depth-mean velocity from the upstream mooring shows predominant variability

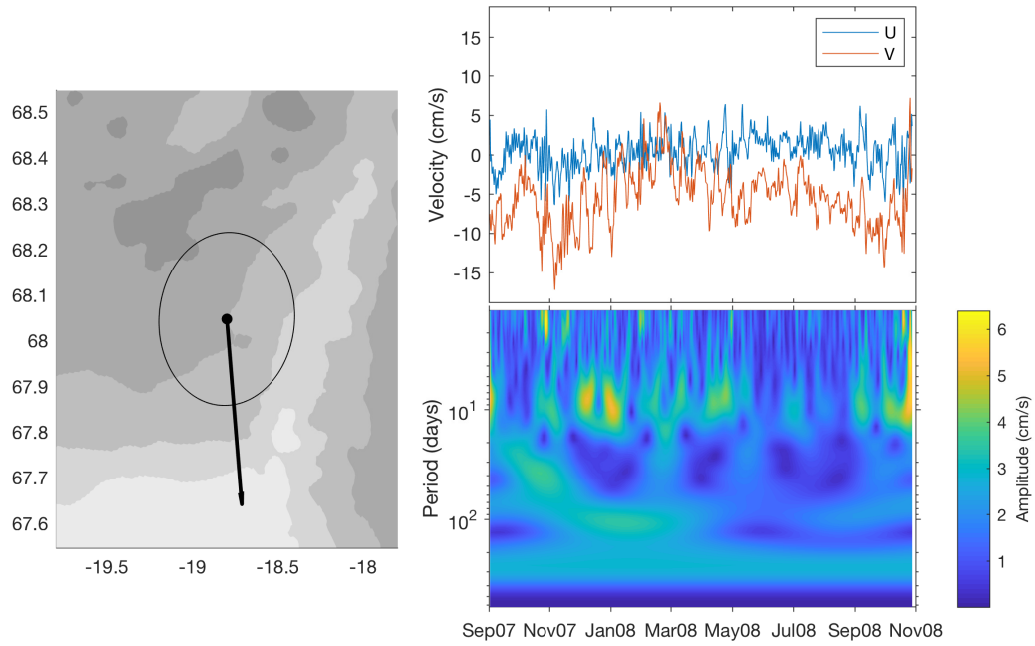


Figure 7: Flow aspects of the depth-mean current from the Kolbeinsey Ridge mooring located approximately 200 km upstream of the Kögur Array. Left: Map showing location of mooring, mean flow (vector) and current ellipse overlaid on the same topography as Figure 4. Right: As Figure 3: time series of the U (blue) and V (red) components of the velocity timeseries (top) and the wavelet spectrum of the velocity field (bottom).

293 at approximately a 10-day period (Figure 7), with much less variability in the 4-day period  
 294 seen in the Kögur Array. As with KGA2–4, the major axis of the current ellipse is at an  
 295 oblique angle to the mean flow, but without additional moorings at this site we are unable  
 296 to assess phase propagation to determine if this variability is consistent with TRWs. How-  
 297 ever, the fact that the TRW inverse ray paths at the Kögur Array do not bend significantly  
 298 upstream, together with the difference in wave frequencies between the sites, suggests that  
 299 the variability at the Kolbeinsey Ridge is not dynamically linked to that at the Kögur Array.  
 300 This supports our assertion that the TRWs at the Kögur Array are locally produced. Inter-  
 301 estingly, the hydrographic data at the Kolbeinsey Ridge mooring (not shown) show clear,  
 302 isolated incursions of EGC water predominantly in the wintertime. This indicates that the  
 303 Separated EGC is active on the Iceland Slope this far upstream of the Denmark Strait sill,  
 304 which implies that if the variability at the Kolbeinsey Ridge mooring is that of TRWs, the  
 305 wave energy there could still potentially be generated by a meandering Separated EGC.

## 306 **4. Summary and Discussion**

307 We have documented the existence of energetic Topographic Rossby Waves (TRWs)  
 308 within the North Icelandic Jet (NIJ) using observations from the densely-instrumented  
 309 Kögur Array located approximately 200 km upstream of the Denmark Strait sill. The  
 310 mean period of the waves is 3.6 days, the wavelength is  $62 \pm 3$  km, and the phase velocity  
 311 is  $17.3 \pm 0.8$  km day<sup>-1</sup> directed downslope ( $-9^\circ\text{T}$ ). Using the TRW dispersion relation,  
 312 we corroborated our observed direction of phase propagation relative to the downslope  
 313 direction ( $24^\circ$ ) with the theoretical value ( $29^\circ$ ). We further determined from the expression  
 314 for group velocity that the wave energy is progressing up-slope ( $138^\circ\text{T}$ ) at 36 km day<sup>-1</sup>,  
 315 in agreement with the observational data. Based on inverse wave tracing, the energy in the  
 316 TRWs appears to emanate locally from the Blosseville Basin. The most likely source is  
 317 the meandering of the offshore Separated East Greenland Current (EGC), although pulses  
 318 of cross-bathymetric flow due to the aspiration of deep overflow water could represent a

319 possible source as well. Winds do not appear to play a role since they vary seasonally  
320 while the TRWs are ubiquitous throughout the year.

321 Notably, our data imply that the dominant high-frequency variability on the Iceland  
322 Slope does not originate from the Denmark Strait, nor does it propagate towards the sill.  
323 This suggests that the mesoscale features at the sill (boluses and pulses), diagnosed obser-  
324 vationally by von Appen *et al.* (2017) and in a model framework by Almansi *et al.* (2017),  
325 are not triggered by, nor directly excite, the TRWs on the Iceland Slope. Nonetheless, the  
326 likelihood of a connection between the high frequency variability at the two locations is  
327 still high given the geographic proximity and the similarity in timescales, but is presum-  
328 ably mediated by another process. The Denmark Strait overflow is believed to be subject  
329 to hydraulic control (Whitehead, 1998; Nikolopoulos *et al.*, 2003), and, consequently, in-  
330 formation should be transferred between the sill and the region to the north, likely as  
331 Kelvin waves. The existence of any such connection and the impact on variability at the  
332 sill and upstream in the EGC and NIJ requires further investigation and is the subject of  
333 an on-going study.

334 Another topic requiring further work is determining where the energy in the TRWs  
335 ends up and what impact it might have on the dynamics of the circulation inshore of the  
336 Iceland slope. Our results indicate that energy is being fluxed into the poleward-flowing  
337 North Icelandic Irminger Current (NIIC), but presently we are unable to say what impact  
338 this has on this current. Våge *et al.* (2011) hypothesize that, to the north of our array, an  
339 offshore flux of warm water associated with the disintegration of the NIIC is tied to the  
340 overturning loop that forms the NIJ. We know that eddies of NIIC water are found both  
341 in the Blosseville Basin (Jónsson and Valdimarsson, 2012) and in the Iceland Sea (Våge  
342 *et al.*, 2011). Future studies of the mechanisms by which the NIIC destabilizes and fluxes  
343 water offshore should take into account the source of energy directed onshore at the Kögur  
344 site and potentially farther north as well on the Iceland Slope.

345 *Acknowledgments.* We would like to thank the crew and technicians aboard the R/V

346 Knorr and RSS James Clark Ross for the deployment and recovery of the Kögur moorings.  
347 This work was supported by National Science Foundation grants OCE-1433958 (BH),  
348 OCE-0959381 (BH and RP) and OCE-1558742 (RP).

349

350

## REFERENCES

- 351 Almansi, M., T. W. N. Haine, R. S. Pickart, M. G. Magaldi, R. Gelderloos, and D. Mas-  
352 tropole. 2017. High-Frequency Variability in the Circulation and Hydrography of the  
353 Denmark Strait Overflow from a High-Resolution Numerical Model. *Journal of Physi-*  
354 *cal Oceanography*, 47(12), 2999–3013. doi: 10.1175/JPO-D-17-0129.1.
- 355 Behrens, E., K. Våge, B. Harden, A. Biastoch, and C. W. Böning. 2017. Composition and  
356 variability of the Denmark Strait Overflow Water in a high-resolution numerical model  
357 hindcast simulation. *Journal of Geophysical Research: Oceans*, 122(4), 2830–2846.  
358 doi: 10.1002/2016JC012158.
- 359 Bruce, J. 1995. Eddies southwest of the Denmark Strait. *Deep Sea Research Part I:*  
360 *Oceanographic Research Papers*, 42(1), 13–29. doi: 10.1016/0967-0637(94)00040-Y.
- 361 Cooper, L. H. N. 1955. Deep water movements in the North Atlantic as a link between  
362 climatic changes around Iceland and biological productivity of the English Channel and  
363 Celtic Sea. *Journal of Marine Research*, 14, 347–362.
- 364 Dickson, R. R. and J. Brown. 1994. The production of North Atlantic Deep Wa-  
365 ter: Sources, rates, and pathways. *J. Geophys. Res.*, 99, 12319–12341. doi:  
366 10.1029/94JC00530.
- 367 Garrett, C. 1979. Topographic Rossby Waves off East Australia: Identification and Role in  
368 Shelf Circulation. *Journal of Physical Oceanography*, 9, 244–253. doi: 10.1175/1520-  
369 0485(1979)009<0244:TRWOEa>2.0.CO;2.

- 370 Harden, B. E., R. S. Pickart, H. Valdimarsson, K. Våge, L. de Steur, C. Richards, F. Bahr,  
371 D. Torres, E. Børve, S. Jónsson, A. Macrandar, S. Østerhus, L. Håvik, and T. Hatter-  
372 mann. 2016. Upstream sources of the Denmark Strait Overflow: Observations from  
373 a high-resolution mooring array. *Deep Sea Research Part I: Oceanographic Research*  
374 *Papers*, 112, 94–112. doi: 10.1016/j.dsr.2016.02.007.
- 375 Håvik, L., K. Våge, R. S. Pickart, B. Harden, W. J. von Appen, S. Jónsson, and S. Øster-  
376 hus. 2017. Structure and variability of the shelfbreak East Greenland Current north of  
377 Denmark Strait. *Journal of Physical Oceanography*, 47, 2631–2646. doi: 10.1175/JPO-  
378 D-17-0062.1.
- 379 Hogg, N. G. 1981. Topographic waves along 70 °W on the continental rise. *Journal of*  
380 *Marine Research*, 39, 627–649.
- 381 Jakobsson, M., L. Mayer, B. Coakley, J. A. Dowdeswell, S. Forbes, B. Fridman, H. Hod-  
382 nesdal, R. Noormets, R. Pedersen, M. Rebesco, H. W. Schenke, Y. Zarayskaya, D. Ac-  
383 cettella, A. Armstrong, R. M. Anderson, P. Bienhoff, A. Camerlenghi, I. Church,  
384 M. Edwards, J. V. Gardner, J. K. Hall, B. Hell, O. Hestvik, Y. Kristoffersen, C. Mar-  
385 cussen, R. Mohammad, D. Mosher, S. V. Nghiem, M. T. Pedrosa, P. G. Travaglini, and  
386 P. Weatherall. 2012. The International Bathymetric Chart of the Arctic Ocean (IBCAO)  
387 Version 3.0. *Geophysical Research Letters*, 39, L12609. doi: 10.1029/2012GL052219.
- 388 Jochumsen, K., M. Moritz, N. Nunes, D. Quadfasel, K. M. H. Larsen, B. Hansen,  
389 H. Valdimarsson, and S. Jonsson. 2017. Revised transport estimates of the Den-  
390 mark Strait overflow. *Journal of Geophysical Research: Oceans*, 122, 3434–3450. doi:  
391 10.1002/2017JC012803.
- 392 Johns, W. E. and D. R. Watts. 1986. Time scales and structure of topographic Rossby  
393 waves and meanders in the deep Gulf Stream. *Journal of Marine Research*, 44, 267–  
394 290. doi: 10.1357/002224086788405356.

395 Jonsson, S. and H. Valdimarsson. February 2004. A new path for the denmark strait over-  
 396 flow water from the iceland sea to denmark strait. *Geophys. Res. Lett.*, *31*(3), L03305–.  
 397 ISSN 0094-8276. URL <http://dx.doi.org/10.1029/2003GL019214>.

398 Jónsson, S. and H. Valdimarsson. 2012. Hydrography and circulation over the southern  
 399 part of the Kolbeinsey Ridge. *ICES Journal of Marine Science: Journal du Conseil*.

400 Käse, R. H., J. B. Girton, and T. B. Sanford. 2003. Structure and variability of the  
 401 Denmark Strait Overflow: Model and observations. *Journal of Geophysical Research:*  
 402 *Oceans*, *108*, 3181. doi: 10.1029/2002JC001548.

403 Lilly, J. M. 2017. jLab: A data analysis package for Matlab, v 1.6.3.

404 Louis, J. P., B. D. Petrie, and P. C. Smith. 1982. Observations of topographic rossby  
 405 waves on the continental margin off nova scotia. *Journal of Physical Oceanography*, *12*,  
 406 47–55. doi: 10.1175/1520-0485(1982)012<0047:OOTRWO>2.0.CO;2.

407 Mastropole, D., R. S. Pickart, H. Valdimarsson, K. Våge, K. Jochumsen, and J. Gir-  
 408 ton. 2017. On the hydrography of Denmark Strait. *Journal of Geophysical Research:*  
 409 *Oceans*, *122*, 306–321. doi: 10.1002/2016JC012007.

410 Mauritzen, C. 1996. Production of dense overflow waters feeding the North Atlantic across  
 411 the Greenland-Scotland Ridge. Part 1: Evidence for a revised circulation scheme. *Deep*  
 412 *Sea Research Part I: Oceanographic Research Papers*, *43*, 769–806. doi: 10.1016/0967-  
 413 0637(96)00037-4.

414 Meinen, C., E. Fields, R. S. Pickart, and D. R. Watts. 1993. Ray tracing on topographic  
 415 rossby waves. Technical Report 93-1, University of Rhode Island.

416 Nikolopoulos, A., K. Borenäs, R. Hietala, and P. Lundberg. 2003. Hydraulic estimates of  
 417 Denmark Strait overflow. *Journal of Geophysical Research: Oceans*, *108*, 3095. doi:  
 418 10.1029/2001JC001283.



- 419 Pedlosky, J. 1979. *Geophysical Fluid Dynamics*. Springer US. doi: 10.1007/978-1-4684-  
420 0071-7.
- 421 Pickart, R. S. 1995. Gulf Stream–Generated Topographic Rossby Waves.  
422 *Journal of Physical Oceanography*, 25, 574–586. doi: 10.1175/1520-  
423 0485(1995)025<0574:GSTRW>2.0.CO;2.
- 424 Pickart, R. S. and D. R. Watts. 1990. Deep Western Boundary Current variability at Cape  
425 Hatteras. *Journal of Marine Research*, 48, 765–791.
- 426 Pickart, R. S., M. A. Spall, D. J. Torres, K. Våge, H. Valdimarsson, C. Nobre, G. W. K.  
427 Moore, S. Jonsson, and D. Mastropole. 2017. The North Icelandic Jet and its relation-  
428 ship to the North Icelandic Irminger Current. *Journal of Marine Research*, 75, 605–639.  
429 doi: 10.1357/002224017822109505.
- 430 Rudels, B., E. Fahrbach, J. Meincke, G. Budéus, and P. Eriksson. 2002. The East Green-  
431 land Current and its contribution to the Denmark Strait overflow. *ICES Journal of Ma-  
432 rine Science: Journal du Conseil*, 59, 1133–1154. doi: 10.1006/jmsc.2002.1284.
- 433 Schultz, R. J., 1987. Structure and propagation of topographic rossby waves northeast of  
434 cape hatteras, north carolina. Master’s thesis, Marine Science Program, University of  
435 North Carolina.
- 436 Smith, P. C. 1976. Baroclinic Instability in the Denmark Strait Overflow.  
437 *J. Phys. Oceanogr.*, 6, 355–371. ISSN 0022-3670. doi: 10.1175/1520-  
438 0485(1976)006<0355:BIITDS>2.0.CO;2.
- 439 Strass, V. H., E. Fahrbach, U. Schauer, and L. Sellmann. 1993. Formation of Denmark  
440 Strait overflow water by mixing in the East Greenland Current. *Journal of Geophysical  
441 Research: Oceans*, 98, 6907–6919. doi: 10.1029/92JC02732.
- 442 Våge, K., R. S. Pickart, M. A. Spall, H. Valdimarsson, S. Jónsson, D. J. Torres, S. Øster-  
443 hus, and T. Eldevik. 2011. Significant role of the North Icelandic Jet in the formation

444 of Denmark Strait overflow water. *Nature Geosci*, 4, 723–727. ISSN 1752-0894. doi:  
 445 10.1038/ngeo1234.

446 Våge, K., R. S. Pickart, M. A. Spall, G. W. K. Moore, H. Valdimarsson, D. J. Torres, S. Y.  
 447 Erofeeva, and J. E. Ø. Nilsen. 2013. Revised circulation scheme north of the Denmark  
 448 Strait. *Deep Sea Research Part I: Oceanographic Research Papers*, 79, 20–39. doi:  
 449 10.1016/j.dsr.2013.05.007.

450 Våge, K., G. W. K. Moore, S. Jónsson, and H. Valdimarsson. 2015. Water mass transfor-  
 451 mation in the Iceland Sea. *Deep Sea Research Part I: Oceanographic Research Papers*,  
 452 101, 98–109. doi: 10.1016/j.dsr.2015.04.001.

453 von Appen, W. J., D. Mastropole, R. S. Pickart, H. Valdimarsson, S. Jónsson, and J. B.  
 454 Girton. 2017. On the nature of the mesoscale variability in denmark strait. *Journal of*  
 455 *Physical Oceanography*, 47, 567–582. doi: 10.1175/JPO-D-16-0127.1.

456 Whitehead, J. A. 1998. Topographic control of oceanic flows in deep passages and straits.  
 457 *Reviews of Geophysics*, 36, 423–440. doi: 10.1029/98RG01014.